FULLY COUPLED NUMERICAL SIMULATION OF A ETHANOL TURBULENT SPRAY FLAME WITH RANS

F. L. Sacomano Filho and G. C. Krieger Filho
fernando.sacomano@gmail.com
Laboratory of Environmental and Thermal Engineering, Polytechnic School, University of São Paulo
Av. Prof. Mello Morais, 2231 - CEP: 05508-030 - São Paulo-SP, Brazil

Abstract
A detailed numerical simulation of ethanol turbulent spray combustion was carried out on a rounded jet flame in a three-dimensional configuration. The focus was on the proposal of a robust mathematical model with relatively low complexity submodels that could well reproduce the main characteristics of the coupling between both phases, like the turbulence modulation, turbulent droplets dissipation and evaporative cooling effect. The results were analyzed and compared to experimental data available in the literature. The simulations were carried out using the Eulerian Lagrangian procedure under a fully two-way coupling. To reproduce the effects of the evaporative cooling the combustion was modeled with a modified flamesheet model with a jointed mixture fraction-enthalpy β-PDF. Reasonable agreement between measured and computed mean profiles of temperature of the gas phase and droplet size distributions was achieved. Some deviations were observed in the mean velocity profiles comparisons between experimental data and simulations, which were assigned to the over predicted diffusion of the mean quantities transported by the gas phase.

1. Introduction
Turbulent liquid spray flames can be found in several industrial combustion systems. The preference for this kind of combustion process is due to three main issues. First, the logistics associated with liquid fuels (transportation and storage) are relatively easier than for gas fuels. Second, turbulent flames, as a whole, allow compact design of combustors. Third, the atomization of the spray, which controls droplet sizes, allows the adjustment of the evaporation process, introducing more flexibility to control the structure of the flame. Nowadays, the interest in the utilization of renewable fuels is increasing. Renewable fuels are being seen as alternatives to fossil fuels to reduce the emission of carbon dioxide among other pollutants. One of the renewable fuels that stands out is the ethanol, mainly due to its wide use in transportation sectors. In this scenario, there is interest on the development of ethanol spray flame investigations for improving performance in engineering devices, such as gas turbine combustors or internal combustion engines.

The study of ethanol turbulent spray flames can be found in empirical investigations, as showed on the works of Marley et al. [1] and Gounder et al. [2], which investigate flames structures. Masri and Gounder [3] studied empirically the behavior of ethanol and acetone spray flames in various regimes of instability and O'Loughlin and Masri [4] analyzed auto-ignition of ethanol and acetone spray flames. Investigations containing also numerical modeling of ethanol turbulent spray flames were showed by Düwel et al. [5], which had as objective the proposition of a spray flame model, by Rochaya [6] which had as objective the modeling of spray flames near to gas turbines operation regimes and, by Ge and Gutheil [7] which continued the work of Düwel et al.

This study aims to propose a robust mathematical model with submodels of relatively low complexity to describe the physics of ethanol turbulent spray flames. For this purpose, the results of the numerical simulations were compared with the experimental data provided by

Masri and Gounder. Numerical simulations were based on RANS turbulence modeling within the Stochastic Separated Flow formulation (SSF). This formulation included submodels for the coupling of all the quantities transported in the gas phase, and the transport phenomena related to droplets and their coupling with the gas phase.

2. Mathematical and numerical modeling

In this section the mathematical and numerical modeling used in this paper are briefly described, further details may be found in Sacomano Filho [8].

2.1. Gas-phase equations

The mathematical modeling in this work was based on the variable density, low-Mach number equations for the gas phase. Any acoustic interactions and compressibility effects were neglected. Despite focusing on steady-state simulation, in the present work the formulation was based on a pseudo-transient approach, which results in the same behavior as under-relaxed steady simulation without modifications in the original code [9]-[10]. Therefore, the equations presented in this section kept the time rate of the transported quantities.

Table 1. Terms of gas phase transport equations.

ψ	D_ψ	S_ψ	$\overline{S_{p,\psi}}$
1	0	0	$\sum_{n=1}^{\alpha}(\Delta m_P/\Delta t)_n/\Delta V$
u_i	$\widetilde{\tau_{ij}} - \bar{\rho}\widetilde{u_i"u_j"}$	$-\frac{\partial \bar{p}}{\partial x_i} + \bar{\rho} g_i$	$\sum_{n=1}^{\alpha}\left[\left(\frac{1}{\tau}(u_{P_i} - u_i) - \frac{g_i(\rho-\rho_l)}{\rho_l}\right)\frac{m_P}{\Delta V} + \overline{S_{p,1}u_{P_i}}\right]_n$
f	$\frac{\mu_t}{\sigma_t}\frac{\partial \tilde{f}}{\partial x_j}$	0	$\frac{s}{s + Y_{ox,0}}\overline{S_{p,1}}$
h	$\frac{\mu_t}{\sigma_t}\frac{\partial \tilde{h}}{\partial x_j}$	0	$\sum_{n=1}^{\alpha}\frac{\left[\left(\frac{m_{Pe}}{Mw_l}\int_{T_{ref}}^{T_{Pe}} c_p dT - \frac{m_{Ps}}{Mw_l}\int_{T_{ref}}^{T_{Ps}} c_p dT - \Delta m_P h_{fl}\right)/\Delta t\right]_n}{\Delta V}$
$f"^2$	$\frac{\mu_t}{\sigma_t}\frac{\partial \widetilde{f"^2}}{\partial x_j}$	$C_g \mu_t \left(\frac{\partial \tilde{f}}{\partial x_j}\right)^2 - C_d \frac{\bar{\rho}\varepsilon}{k}\widetilde{f"^2}$	$\frac{\widetilde{f"^2}(1-2\tilde{f})}{\tilde{f}}\overline{S_{p,f}}$
k	$\frac{\mu_t}{\sigma_k}\frac{\partial k}{\partial x_j}$	$2\mu_t \widetilde{S_{ij}}\cdot\widetilde{S_{ij}} - \bar{\rho}\varepsilon$	$\overline{u_i S_{ui}} - \bar{u}_i\overline{S_{ui}} + \frac{1}{2}\left(\overline{u_i{}^2 S_{p,1}} - \overline{u_i{}^2 S_{p,1}}\right)$
ε	$\frac{\mu_t}{\sigma_\varepsilon}\frac{\partial \varepsilon}{\partial x_j}$	$C_{1\varepsilon}\frac{\varepsilon}{k}2\mu_t\widetilde{S_{ij}}\cdot\widetilde{S_{ij}} - C_{2\varepsilon}\bar{\rho}\frac{\varepsilon^2}{k}$	$C_{3\varepsilon}\frac{\varepsilon}{k}\overline{S_{p,k}}$

The gas phase was the continuum phase and was modeled with the Favre averaging method. Equation (1) presents the transport equation for a general variable ψ, which was used to calculate the transport of gas phase quantities.

$$\frac{\partial \bar{\rho}\tilde{\psi}}{\partial t} + \frac{\partial \bar{\rho}\tilde{\psi}\tilde{u_j}}{\partial x_j} = +\frac{\partial}{\partial x_j}\left(D_\psi\right) + S_\psi + \overline{S_{p,\psi}}\,, \tag{1}$$

where, $\bar{\rho}$ is the time averaged density of the gas mixture, t is the time, x_j is the spatial Cartesian coordinate in j direction, $\widetilde{u_j}$ is the density-weighted averaging of the Cartesian component of velocity in j direction, D_ψ is the diffusive part of the equation, S_ψ is related to extra and source terms of the equation and $\overline{S_{p,\psi}}$ is the source term associated with the transport and evaporation of droplets. This last term made the coupling of the gas to the disperse phase.

The physical quantities transported by the gas phase correspond to mass, momentum, mixture fraction (f), specific enthalpy (h), mixture fraction variance (f''^2), kinetic turbulent energy (k) and dissipation of kinetic turbulent energy (ε). The terms D_ψ, S_ψ and $\overline{S_{p,\psi}}$, of each one of these physical quantities are presented in Table 1. It is worthy to note the terms $\overline{S_{p,\psi}}$ are presented in Table 1 in their respective discretized form.

m_P is the mass of a droplet and Δm_P its variation due to the evaporation, ΔV is the volume of a cell, Δt is the time step of dispersed phase and α is the total number of particles in a cell in the time step of the continuous phase. In the equation of momentum, i.e. the equation illustrated by the variable u_i in Table 1, the terms $\widetilde{\tau_{ij}}$ and $\bar{\rho}\widetilde{u_i''u_j''}$ are related to mean flow stress and Reynolds stress tensors, respectively. Both of them are respectively expressed by Eqs. (2) and (3).

$$\widetilde{\tau_{ij}} = 2\mu\widetilde{S_{ij}} - \frac{2}{3}\delta_{ij}\left(\mu\frac{\partial\tilde{u}_k}{\partial x_k}\right), \tag{2}$$

$$-\bar{\rho}\widetilde{u_i''u_j''} = 2\mu_t\widetilde{S_{ij}} - (2/3)\bar{\rho}k\delta_{ij}\,, \tag{3}$$

where, μ is the molecular viscosity, $\widetilde{S_{ij}}$ is the deformation tensor, which is given by $\widetilde{S_{ij}} = 1/2\left(\partial\widetilde{u_i}/\partial x_j + \partial\widetilde{u_j}/\partial x_i\right)$, δ_{ij} is the Kronecker's delta operator, u_j'' is the density-weighted component of turbulent fluctuation of the velocity in direction j, μ_t is the turbulent viscosity, which can be written as $\mu_t = \bar{\rho}C_\mu\, k^2/\varepsilon$. C_μ , as well as σ_k, σ_ε, $C_{1\varepsilon}$, $C_{2\varepsilon}$, is an adjustable constant of the k-ε Standard model; they have the values of 0.09, 1.00, 1.30, 1.44 and 1.80, respectively, in this model. Yet in momentum equation, g_i is the i component of the gravity acceleration, $\bar{p}$ is the pressure, τ is the relaxation time scale of a droplet, which is pointed in Eq. (5). u_{P_i} is the instantaneous component of velocity in i direction of the droplet, g_i is the component in the i direction of the gravitational acceleration, ρ_l is the density of the liquid phase.

In the mixture fraction equation, the variable σ_t is the turbulent Prandtl/Schmidt number, which had the value of 0.85 in this work, s is the stoichiometric oxidant/fuel mass ratio for the global reaction mechanism and $Y_{ox,0}$ is the maximum mass fraction of oxidant in flame domain. The subscripts index $(.)_e$ and $(.)_s$ used for the mass and temperature (T_p) of the particle, in source terms associated to droplets in energy equation, are related to these properties when a particle respectively enters or exits a cell. Also in energy equation, Mw_l is the molecular weight of the liquid, T_{ref} is a reference temperature, c_p is the sensible specific heat and h_{fl} is the enthalpy of vaporization of the fuel.

The adjustable constants C_d and C_g defined in the equation of mixture fraction variance have respectively the values 2.00 and 2.80. In the equation of ε the term $C_{3\varepsilon}$ in the source term associated to droplet transport and evaporation is an adjustable parameter that is derived from experimental data and depends on droplet diameter distribution and dispersed phase

concentrations [11]. Hollman and Gutheil [12] found the value of 1.0 in their studies with spray flames in free air and Chrigui [11] found the value of 1.87 fitted very well to his measurements. However, in this work the value 1.15 was used to this parameter, which allowed more agreement between the simulation results and experimental data.

It is worthy to notice the source terms associated with the transport and evaporation of droplets have the same formulation given in Chrigui et al. [13], except for the mixture fraction and its variance. The source term of the mixture fraction variance is the same used in Chrigui et al. [14].

All of the gas flow equations were solved with the Finite Volume Method, on which the pressure-velocity coupling was done with the Pressure Implicit and Momentum Explicit (PRIME) scheme [10]. A second-order Total Variation Diminishing (TVD) scheme with the SUPERBEE limiting function [9] is used for advective terms and centered differencing for the diffusive terms. Once the simulation is pseudo-transient, all terms, except for the inter-phase source terms, are treated implicitly using first order Euler method for temporal discretization.

2.2. Liquid-phase equations

Droplet entrainment was calculated with the SSF method [15], which uses a Lagrangian point-particle model. This method accounts for the coupling of the turbulence between the phases for the turbulence dispersion of droplets, as for the effects of the presence of particles in the gas phase. The equations of droplets were modeled in a Lagrangian coordinate system, where they are treated as discrete points in the gas flow. The equations of droplet movement can be written as:

$$\frac{d\overrightarrow{x_p}}{dt} = \overrightarrow{u_p}\,, \tag{4}$$

$$\frac{d\overrightarrow{u_p}}{dt} = \underbrace{\left(\frac{18\mu}{d_p^2\rho_l}\frac{C_D Re_e}{24}\right)}_{\tau}\left(\vec{u} - \overrightarrow{u_p}\right) + \frac{\vec{g}(\rho_l - \rho)}{\rho_l}\,, \text{where } Re_e = \frac{\rho d_p\left|\vec{u} - \overrightarrow{u_p}\right|}{\mu}, \tag{5}$$

and, $\overrightarrow{x_p}$ and $\overrightarrow{u_p}$ are respectively the displacement and the instantaneous velocity vector of the droplet, $\vec{u}$ is the instantaneous velocity vector of the gas phase and $\vec{g}$ is the gravity acceleration vector. Other droplets characteristics are: d_p is its diameter, Re_e is its Reynolds number and C_D is its draft coefficient, which was given by the correlation recommended in Yuen and Chen [16] and can be written as:

$$C_D = \begin{cases} \dfrac{24}{Re_e}\left(1 + \dfrac{Re_e^{\,2/3}}{6}\right) : 0 < Re_e < 1000 \\ 0.44 : \qquad Re_e \geq 1000 \end{cases}. \tag{6}$$

The droplet evaporation is modeled based on a two-stage model [15], in which, in a first stage, the mass transfer of the droplet is driven by the difference in fuel vapor concentration between the surface of the droplet and its surroundings until the droplet reaches the boiling point temperature when the rate becomes driven by the difference of temperatures. In the second stage, the temperature of the droplet is constant. Droplet heating is modeled by the infinite-liquid-conductivity model [17], in which there is a spatially uniform but time-varying droplet temperature.

The Lagrangian equations governing droplet temperature and mass for the first stage were:

$$m_p c_p \frac{dT_p}{dt} = hA_p\left(T - T_p\right), \tag{7}$$

where, c_P is the specific sensible heat of the liquid, T_P is the temperature of the droplet, T is the temperature of the gas phase, A_P is the surface area of the droplet and h is the heat transfer coefficient of convection, which is given by the correlation for the Nusselt number (Nu) of Ranz and Marshall [18]. The equation of this Nu and the Ranz and Marshall Sherwood number (Sh) [18], are presented in Eq. (9). For this stage the mass transfer is driven by:

$$\frac{dm_p}{dt} = -k_C\left(C_{l,s} - C_{l,\infty}\right)A_p Mw_l \text{ , in which: } C_{l,s} = \frac{p_{sat}\left(T_p\right)}{T_p R_u} \text{ and } C_{l,\infty} = \frac{X_i p}{T \cdot R_u}. \tag{8}$$

$$Sh = \frac{k_C d_p}{D_{l,m}} = 2{,}0 + 0{,}6{Re_e}^{1/2}Sc^{1/3} \text{ and } Nu = \frac{hd_p}{k_\infty} = 2{,}0 + 0{,}6{Re_e}^{1/2}Pr^{1/3}. \tag{9}$$

k_C is the mass transfer coefficient, $C_{L,S}$ is the concentration of liquid vapor on surface of the droplet, $C_{L,\infty}$ is the concentration of liquid vapor on gas phase, p_{sat} is the saturation pressure of the liquid, X_L is the mole fraction of the liquid vapour, p is the gas pressure, R is the universal constant of ideal gases, $D_{L,m}$ is the binary mass diffusion coefficient of vapour of the liquid in air, Sc is the Schmidt number, k_∞ is the thermal conductivity of the gas phase and Pr is the Prandtl number.

The second stage equations are:

$$\frac{dd_P}{dt} = \frac{2}{h_{fl}\rho_l}\left[\frac{Nu \cdot k_\infty}{d_P}\left(T - T_P\right)\right] \tag{10}$$

$$Nu = \frac{ln(1+B)}{B}\left(1 + 0.39Pr^{1/3}Re^{1/2}\right), \qquad B = \frac{c_P}{h_{fl}}\left(T - T_P\right) \tag{11}$$

Here, B is the Spalding number [19].

All of these equations that describe the dynamics of droplets processes were discretizated with the Explicit Euler Method, except for the equations of droplet entrainment, which were discretized with the Implicit Euler Method.

The turbulence coupling of the disperse phase to the gas phase was done with the modeling of the turbulent dispersion of droplets. To reproduce the turbulent dispersion of droplets in this work, the stochastic random walk model presented in Faeth [15] was used. The analysis made in Faeth indicates stochastic methods as a good alternative to reproduce this kind of dispersion. Stochastic methods involve particle dispersion directly.

2.3. Combustion modelling

For the present study, the chemical reactions are modeled with a modified flamesheet model with a joint mixture fraction-enthalpy β-PDF. The original flamesheet model [20] is an adiabatic combustion model, and for that reason this original model does not allow the modeling of the evaporative cooling effect. Hence, a modification was done in this model to account for this effect. When droplets evaporate, they remove sensible heat of the gas flow. What was done in the modified model was the consideration of a limiting condition in relation to the original model, in which another table of enthalpy of the mixture was made considering

all the fuel mass present in the mixture came from the evaporation process. As a result, other tables of temperature and density were obtained. It is worthy to notice that the reaction was modeled as in the adiabatic form, so no changes in reaction rate were accounted for the presence of the evaporative cooling effect.

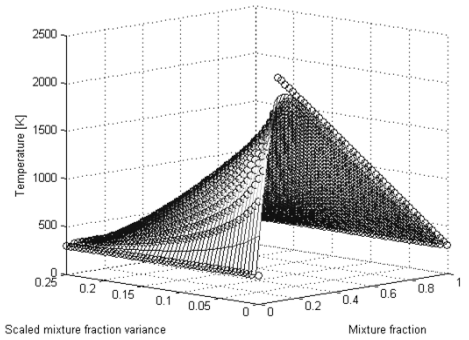

Figure 1. Pre-integrated adiabatic β-PDF.

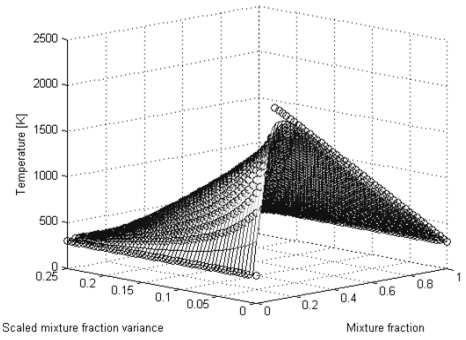

Figure 2. Pre-integrated non adiabatic β-PDF.

With this new modified flamesheet model a joint mixture fraction-enthalpy β-PDF was obtained. In this approach it was considered the conditional PDF on enthalpy [$\tilde{P}(f,h) = \tilde{P}(f|h) = \tilde{P}(f) \cdot \tilde{P}(h)$, where $\tilde{P}(\psi)$ is the PDF function of ψ], in which the PDF of the enthalpy was modeled as a Dirac delta function, $\tilde{P}(h) = \delta(h - \tilde{h})$. With this consideration, two tables of the β-jointed PDF were calculated, one adiabatic and another in the limiting condition of the modified flamesheet model. When the simulation is running the properties that come from the reaction are interpolated between these two tables, which are shown in Figs. 1 and 2. The scaled mixture fraction is given by $\widetilde{f''^2_{sc}} = 0.25\ \widetilde{f''^2}/[\tilde{f}(1-\tilde{f})]$.

The liquid droplets evaporate and the resulting fuel vapor mixes with the surrounding gas and combustion takes place in the gas phase. Surface reactions in droplets and envelope flames were not regarded in this work.

3. Boundary conditions

The experimental data used in this work was extracted from the work of Masri and Gounder. In this experimental work measurements of mean temperature for the gas phase, and axial mean velocity, turbulent axial velocity fluctuations and size distributions of droplets in pilot-stabilized jet flames of dilute sprays of ethanol and acetone were reported. However, in this present work only the ethanol flame Etf3 was analyzed.

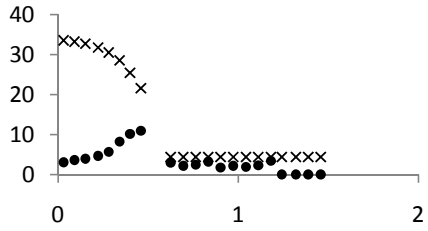

Figure 3. Bc's for axial velocity (x) and its turbulent fluctuations (●) in m/s

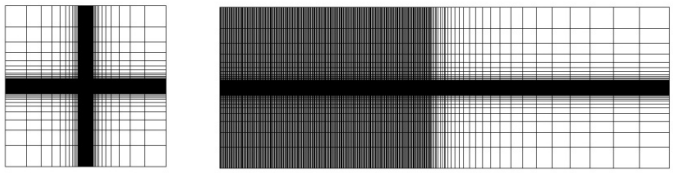

Figure 4. Top and side view of the computational grid

To proceed with the simulations, the inflow boundary conditions (bc) for velocity were linearly interpolated onto the grid from the data of Fig. 3. For the other physical quantities, except for pressure, the boundary conditions are also of Dirichlet type. The inflow bc for

mixture fraction had the value of 0.12 in the nozzle exit and null in the remaining inflow cross section. For k and ε the Eq. (12) was used. Pressure boundary condition in the injection face was not prescribed, because, in the PRIME scheme, the values of velocities used as boundary conditions do not need to be corrected. On the other boundaries of the domain a Dirichlet type with null was prescribed for pressure, and a Neumann type with null value for the other quantities.

$$k = \sqrt{u"_i u"_i/2} \text{ and } \varepsilon = C_\mu^{3/4} k^{3/2}/0.07L\,, \tag{12}$$

where L is the turbulent integral scale defined as the radius of the nozzle diameter.

The bc's for droplets are taken directly from experimental measurements. Once achieved the droplet distribution curves, a random launcher was used. It launches these quantities one by one. With this scheme, almost a thousand particles are launched per time step.

Figure 4 shows the grid used in the numerical simulations. The domain size had dimensions of 37*D* x 37*D* x 98*D* with *D* being the diameter of the fuel nozzle (10.5 mm). The Cartesian grid has a size of 1,837,368 cells that was composed by 78 x 78 x 302 grid nodes in the both transversal directions (x, y) and in the longitudinal direction (z), respectively. For the first 47*D* in the z direction the grid is equidistant; downstream of that zone, the grid points are linearly expanded with an expansion ratio of 1.12. In the x and y directions, the grid points are uniformly spaced with 3*D*, from the center line of the jet to its boundaries, and the adjacent space was completed with a linearly expansion ratio of 1.3.

4. Results and discussion

The code used in this work was developed originally for LES by Fukumasu [21], which also validated its operation. Changes were done in [8] to implement the k-ε Standard turbulence model and the disperse phase modeling. This code was based on a finite-volume method to solve the low-Mach number, variable density gas-phase flow equations on Cartesian grids with the co-located scheme. OpenMP™ parallel processing method was applied to the solver, improving computation speed in 4 times.

The results were collected when the solution was considered converged, which means almost 40,000 iterations. The convergence was determined when the results did not presented significant change with iterations advancement and the residuals of gas transport equations were low. The overall computational time was less than 500 CPU-hours on a SGI® Altix® XE320 with 16 processors.

Comparisons between experimental data and numerical simulations results were done at three cross sections (z/D = 10, 20 and 30) for gas phase mean excess temperature and droplet axial mean velocities for five size ranges of droplets diameters, which are respectively presented by Figs. 5 and 6. In Fig. 5 is also presented a comparison between experimental data and simulation results in the cross section of z/D = 0.3, which is actually a boundary condition for droplet's velocities.

Observing the results of the simulations presented at the cross section 10*D* far from the nozzle, in Fig. 5, it can be noted a relative good agreement to the experimental data of the axial mean velocities in the region near to the spray jet centerline for all droplet's size ranges. However, an increasing disagreement toward the border of the spray jet can be observed in this same cross section. A similar behavior is shown at the respective graphic of a 20*D* axial distance from the nozzle. This behavior can be addressed to a higher diffusion in the radial direction in the gas phase velocities of numerical simulation than in the experimental spray flame, which reduces the velocity of the droplets. At the same time, this radial diffusion seems to disappear in the axial distance of 30*D* from the nozzle, in which there is not a

pronounced decay of droplets mean axial velocities in the radial direction. However, this behavior is similar to the observed in experimental data at this same cross section.

Fig. 5 also shows that simulated droplet's velocities are lower than droplets measured velocities in all four cross sections. This disagreement increases as the axial distance from the nozzle increases. This behavior was assigned to the turbulence modeling, specifically to the turbulence modulation modeling, which will be discussed later in this topic.

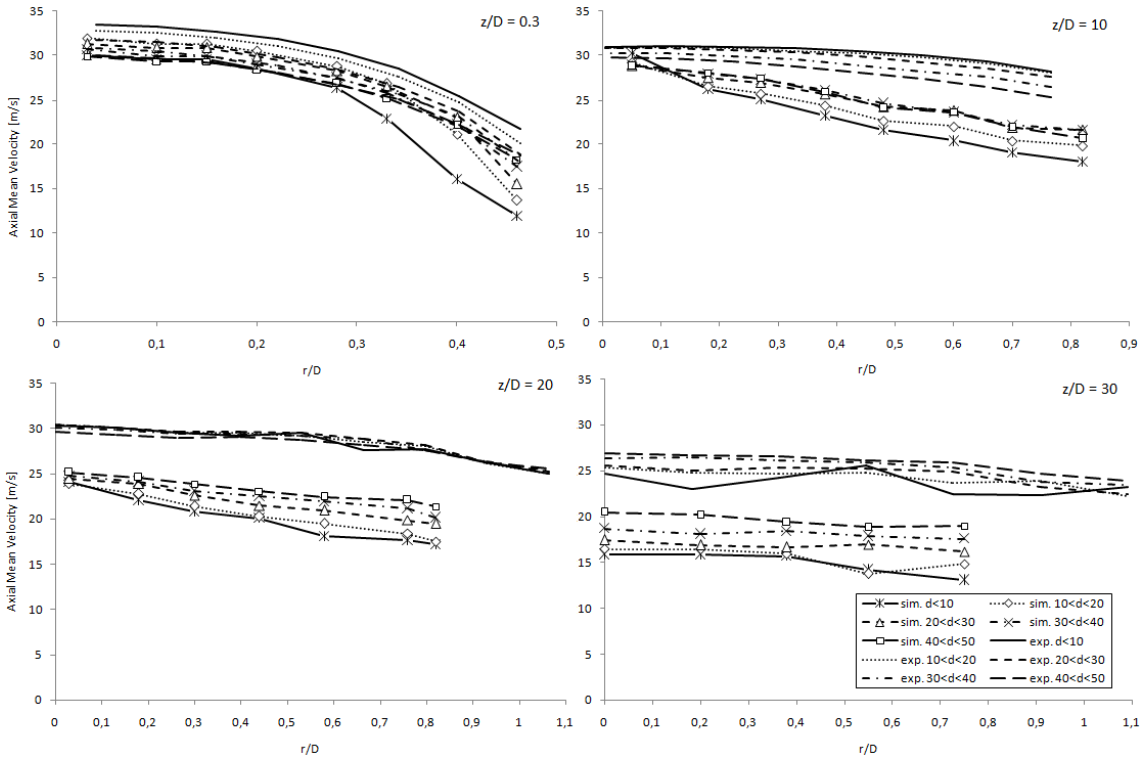

Figure 5. Radial profiles of droplet mean axial velocities

It is worth to notice small droplets have low inertia compared to bigger ones, which means that small droplets have shorter relaxation time scales (τ) than large droplets [this last statement can be deduced by the τ expression, presented in eq. (5)]. Thus, large droplets keep their own dynamics through the flow field while small ones (in this case, droplets smaller than 10 µm) accompany the gas flow. So, small droplets are more affected by the dispersant phase than large ones. From these observations and analyzing only the experimental data in Fig. 5, it can be verified that, in regions near to the nozzle, the gas flow velocities were larger than overall droplets' velocities. Nonetheless, the axial mean velocities of gas and dispersed phase are almost the same at an axial distance of 20*D* from the nozzle, moreover the scenario observed in the early spray inverts at the cross section of *z/D* = 30. This overall behavior observed for the experimental spray was not the same for the simulation results. Actually, larger droplets still always with larger velocities than small ones in all the flow field as was shown in Fig. 5, except for the region near to the spray jet centerline in cross section of *z/D* = 10, which indicates that the dispersant phase had lower velocities in axial direction in simulations than in the experiment.

Despite these low velocities verified in simulations, mean temperature radial profiles of gas phase velocities showed good agreement in short distances from the nozzle. Observing the results presented by Fig. 6, up to a distance of 20*D* from the nozzle, the mean temperature

field of gas phase accompanied the experimental measurements with low discrepancies. Nevertheless, the simulation results presented a more pronounced radial diffusion than the experimental data, which can be easily noted by the smooth decay of the curve from the highest to low temperatures. The radial profile of the *z/D* = 30 cross section shows more pronounced discrepancies than the last two ones. At this region higher temperatures are reached by the simulation than by the experiment. Before discussing the effects that eventually promoted these discrepancies in the simulated flame, it is worthy to observe the comparison between droplets size distribution presented in Fig. 7.

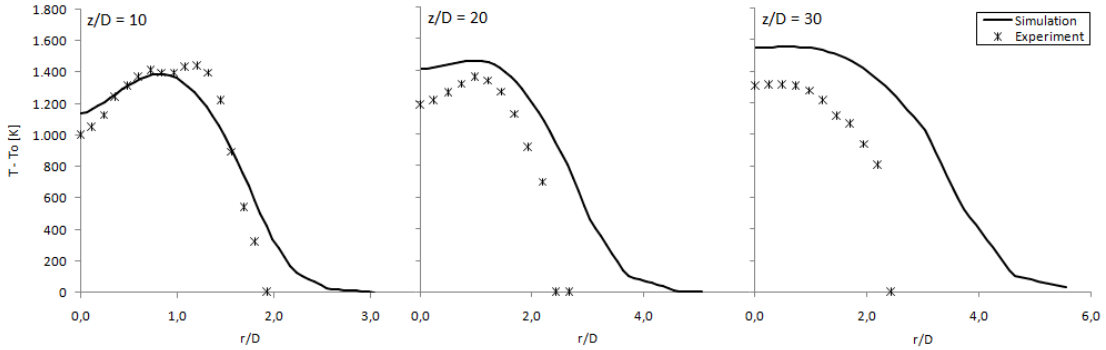

Figure 6. Radial profiles of gas mean excess temperature in axial distances from the nozzle of 10*D*, 20*D* and 30*D*, respectively.

Observing the results in Fig. 7 it can be noted that the numerical simulations well reproduced droplet size distributions throughout the flow field. Some discrepancies are shown at point 10 *z/D*, *r/D* 0.05, in which the simulation concentrates on larger droplets than the experiment. This is assigned to the fact these droplets just passed through a region of high temperatures, which is found near to the nozzle, where the mixture fraction reached its stoichiometric value. The points 10 *z/D*, *r/D* 0.71 and 10 *z/D*, *r/D* 0.82 in Fig. 7 showed a concentration of small droplets slightly more pronounced than in experiment measurement. These discrepancies are explained by the fact that the droplets acquired at this point had passed through a region of high temperatures in regions near to nozzle. As a result, these discrepancies reflect disagreements in the combustion modeling, which gives higher temperatures in some regions than in the experimental flame.

From the results shown by Figs. 6 and 7 it can be concluded the evaporation process and the turbulent dispersion of droplets were well predicted by the simulation. Observing the results of Fig. 5 it could be noted that difference of velocities between the gas phase flow and disperse phase do not affect effectively the evaporation model. The difference between velocities was over predicted by simulations. When the results from Fig. 5 are related to the equations of Nusselt number (Eqs. 9 and 11) that depends on the Re_e and, this last to the difference of velocities between liquid and gas phase, it can be noted that this non-dimensional number was over predicted in simulations. Therefore, considering the well predicted droplet's size distributions and the good agreement between simulated and measured temperatures of the gas phase, one can notice that the difference between velocities do not affect effectively the evaporation model. Bearing in mind that the reduction of size of droplets results from the mass transfer that happens when droplets move through the flow field, at the compared points presented in Fig. 7 (which are taken until an axial distance of 30*D* from the nozzle) the major contribution to droplet's evaporation comes from the well predicted part of the temperature field. Thus, the over predicted temperatures at the *z/D* = 30 cross section did not contribute effectively to the measured droplet's size distributions.

The over predicted temperatures at an axial distance of 30*D* from the nozzle in Fig. 6 were addressed to the combustion model utilized. Despite the evaporation process was regarded in the present work, which makes the flamesheet model non-adiabatic, the chemical reaction mechanisms of ethanol were represented in this model by an irreversible global reaction. Hence, the reaction taxes, which control the realization of sensible enthalpy to the flow, were not accounted.

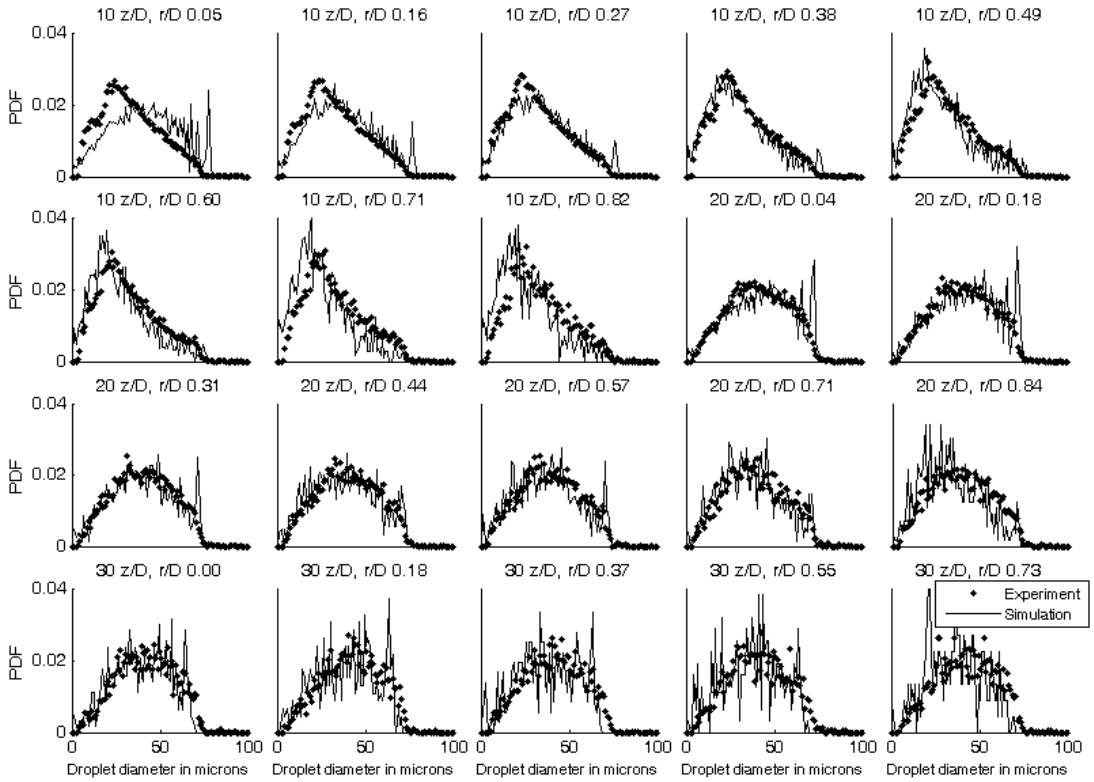

Figure 7. Probability Density Functions of droplets size distributions.

The low velocities observed in the simulation results were addressed to an over predicted turbulent viscosity in the dispersant phase. Even though the velocities of injection of droplets were underestimated as is shown in cross section z/D = 0.3 in Fig. 5 (which is assign to problems in the stochastic launcher), the increasing reduction of velocities as the axial distance increases is addressed to problems in turbulence modeling.

In the validation of the numerical code used in this work, which is presented in [8], numerical simulations well predict a monophasic round jet diffusion flame. In this validation the parameter $C_{2\varepsilon}$ was changed to 1.80 to account for the round jet anomaly [22], as was done by Chen et al. [23]. As a result, the turbulent diffusion over predicted in this study is assigned to the turbulence modulation modeling, which accounts for the effects of droplets dynamics over the gas phase turbulence. Chrigui [11] mentioned the Standard turbulence modulation model over predicts the turbulence and recommends the use of the Thermodynamically Consistent model to improve the modeling. Despite this finding, one difficulty is to define the parameter $C_{3\varepsilon}$. Squires and Eaton [24] presented a relation between this parameter with particle mass loading and relaxation time scale, although they mentioned that considering the existence of a wide range of values for the parameter $C_{3\varepsilon}$, its value is usually obtained by

tuning to yield a good agreement with a particular laboratory experiment. These authors also presented that the parameter $C_{2\varepsilon}$ changes its value according to the mass loading and droplet's relaxation time scales. Therefore, further studies evaluating other turbulence modulation modeling and the adjustment of k-ε equation's parameters according to the characteristics of the spray will be required to improve the simulation results obtained in this work.

5. Summary and conclusions

In this work, simulations of an ethanol turbulent spray flame in an open air combustor under the conditions corresponding to an experiment by Masri and Gounder [3] were performed. An Eulerian–Lagrangian formulation was applied to calculate the development of the spray. The variable density, low-Mach number equations for reacting turbulent flows with phase changing due to droplet evaporation were solved on a tridimensional Cartesian mesh. The droplet dynamics was modeled using the SSF approach and an infinite-liquid-conductivity model for evaporation.

The coupling between the phases was fully done. The turbulence dispersion of droplets was calculated with a random walk model and the turbulence modulation was modeled with the model used in [13]. The combustion modeling was one with a modified flamesheet modeling, since the statistical treatment for the turbulent reactions was done with a jointed mixture fraction-enthalpy β-PDF approach.

Comparisons between the computed and measured axial mean velocity of different droplets size ranges and mean temperature of the gas phase were done. Some discrepancies were observed in the velocities of droplets which were addressed to the over predicted diffusion of the gas flow, which was consequently assigned to the adopted turbulence model. Relative good agreement of gas phase temperatures are obtained for regions near to the nozzle, although some discrepancies were observed in regions far form then, which are addressed to the combustion modeling.

Good agreement was observed to droplet size distributions. These results showed that, in spite of some discrepancies observed in the gas flow results, the evaporation of the spray was well reproduced. However some implications of the discrepancies of the gas phase calculation could be observed in the droplet size distributions.

Therefore, modifications in the turbulence modulation modeling and adjustment of k-ε turbulence model constants are expected to improve the results of the calculated gas flow quantities in a future work.

6. Acknowledgements

The authors would like to thank the Coordenação de Aperfeiçoamento de Pessoal de Nível Superior (CAPES) for supporting of this work under the grant ''CAPES-PRÓ-ENGENHARIAS / ESTUDO COMPUTACIONAL E EXPERIMENTAL DE CHAMAS TURBULENTAS DE ETANOL''- PE004/2008 and, the Laboratory of Environmental and Thermal Engineering (LETE) of the Polytechnic School of the University of Sao Paulo.

7. References

[1] Marley, S. K., Welle, E. J., Lyons, K. M., Roberts, W. L., "Effects of leading edge entrainment on the double flame structure in lifted ethanol spray flames", *Exp. Thermal & Fluid Sci*. 29: 23-31 (2004)

[2] Gounder, J. D., Starner, S. H., Masri, A. R., "Effects of Droplet Loading in Turbulent Spray Ethanol Flames", *Fourth Australian Conference on Laser Diagnostics in Fluid Mechanics and Combustion*. pp. 49-52 (2005)

[3] Masri, A. R., Gounder, J. D., "Turbulent Spray Flames of Acetone and Ethanol Fuels Aproaching Extintion". *Proc. of MCS6* (2009)

[4] O'Loughlin, W., Masri, A. R., "A new burner for studying auto-ignition in turbulent dilute sprays", *Comb. & Flame*. (Article in press)
[5] Düwel, I., Ge, H.-W., Kronemayer, H., Dibble, R. Gutheil, E., Schulz, C., Wolfrum, J., "Experimental and numerical characterization of a turbulent spray flame", *Proc. Comb. Inst.*. 31: 2247-2255 (2007)
[6] Rochaya, D., *Numerical Simulation of Spray Combustion using Bio-mass Derived Liquid Fuels*, PhD. Thesis, 2007, 292p.
[7] Ge, H.-W., Gutheil, E., "Joint PDF Modeling of Non-reacting and Reacting Turbulent Spray Flows", *Proc. 19th National & ISHMAT-ASME Heat and Mass Transfer Conference*, paper UG-017, pp. 1-10 (2008)
[8] Sacomano Filho, F. L., *Simulações de chamas turbulentas de spray de etanol com modelo de turbulência k-ε*, Master of Sciences dissertation, 2011 *no prelo*.
[9] Versteeg, H. K. and Malalasekera, W., *An Introduction to Computational Fluid Dynamics: The Finite Volume Method*, Pearson Education Limited, 2007, 503p.
[10] Maliska, C. R., *Transferência de calor e mecânica dos fluidos computacional*, Livros Técnicos Científicos Editora, 2004, 453p.
[11] Chrigui, M., *Eulerian-Lagrangian Approach for Modeling and Simulations of Turbulent Reactive Multi-Phase Flows under Gas Turbine Combustor Conditions*, Dr. –Ing. Thesis, 2005, 160p.
[12] Hollmann, C., Gutheil, E., "Flamelet-Modeling of Turbulent Spray Diffusion Flames Based on a Laminar Spray Flame Library", *Comb. Sci. & Tech.* 135: 175-192 (1998)
[13] Chrigui, M., J., Hage, M., Dreizler, Sadiki, A., Janicka, A., "Experimental and Numerical Analysis of Spray Dispersion and Evaporation in a Combustion Chamber", *Atom. & Sprays*. 19: 929-955 (2009)
[14] Chrigui, M., Moesl, K., Ahmadi, W., Sadiki, A., Janicka, J., "Partially premixed prevalorized kerosene spray combustion in turbulent flow", *Exp. Thermal & Fluid Sci*. 34: 308-315 (2010)
[15] Faeth, G. M., "Evaporation and combustion of sprays", *Prog. Energy Combust. Sci*. 9: 1-76 (1983)
[16] Yuen, M. C., Chen, L. W., "On Drag of Evaporating Liquid Droplets", *Comb. Sci. & Tech.* 14: 147-154 (1976)
[17] Sirignano, W. A., *Fluid Dynamics and Transport of Droplets and Sprays*, Cambridge University Press, 2010, 462p.
[18] Incropera, F. P., DeWitt, D. P., *Fundamentos de transferência de calor e de massa*, LTC – Livros Técnicos e Científicos Editora S. A., 2003.
[19] Kuo, K. K., *Principles of Combustion*, John Wiley & Sons, Inc., 1986, 810p.
[20] Turns, S. R., *An introduction to combustion: concepts and applications*, McGraw-Hill series in mechanical engineering, 2000, 676p.
[21] Fukumasu, N. K., *Modelagem de uma chama de difusão turbulenta pela simulação das grandes escalas*, MSc. Thesis, 2010, 119p.
[22] Pope, S. B., "An Explanation of the Turbulent Round-Jet/Plane-Jet Anomaly", *AIAA Journal*. 16: 279-281 (1978)
[23] Chen, J. –Y., Yam, C., Armstrong, R., "Joint Scalar PDF Simulation of Turbulent Reacting Flows with Detailed Chemistry on a Parallel Cluster", in: *Proc. of TNF4* (1999)
[24] Squires, K. D., Eaton, J. K., "Effect of Selective Modification of Turbulence on Two-Equation Models for Particle-Laden Turbulent Flows", *ASME J. Fluids Eng.* 116: 778-784 (1994)